

Plane-waves DFT-LDA calculation of the electronic structure and absorption spectrum of Copper

Andrea Marini, Giovanni Onida and Rodolfo Del Sole

Istituto Nazionale per la Fisica della Materia, Dipartimento di Fisica dell'Università di Roma "Tor Vergata", Via della Ricerca Scientifica, I-00133 Roma, Italy
(October 25, 2018)

We present an accurate, first-principles study of the electronic structure and absorption spectrum of bulk copper within Density Functional Theory in the Local Density Approximation (DFT-LDA), including the study of intraband transitions. We construct norm-conserving pseudopotentials (PPs) including the 3d shell (and optionally the underlying 3s and 3p shells) in the valence, and requiring a relatively small plane-waves basis (60 and 140 Rydbergs cutoff, respectively). As a consequence, these PPs are strongly non-local, yielding to macroscopically wrong results in the absorption spectrum when momentum matrix elements are computed naively. Our results are compared with experimental photoemission, absorption and electron energy loss data, and suggest non trivial self-energy effects in the quasiparticle spectrum of Cu.

78.40.Kc 71.15.Dx 71.20.-b 78.20.-e

I. INTRODUCTION

Copper has played for a long time a central role in the elucidation of the electronic structure of solids. It is a relatively inert material, very easy to handle experimentally; its energy dispersion relations (including spin-orbit interaction for some bands) have been measured with considerable precision; lifetimes of the band states as a function of the distance from Fermi level have been determined; surface states have been analyzed in various parts of Surface Brillouin zone (for a review see¹). From the theoretical side, the study of noble metals like Copper using first-principles methods based on plane-waves and ab-initio pseudopotentials (PPs) presents some peculiar complication with respect to the case of simple metals or semiconductors. In fact, in addition to metallicity, which implies the use of an accurate sampling of the Brillouin zone in order to describe properly the Fermi surface, one must also keep into account the contribution of d-electrons to the bonding and to the valence band-structure. This means that, within the PP scheme, d states cannot be frozen into the core part, but must be explicitly included into the valence, yielding a large total number of valence electrons (11 for bulk copper). Unfortunately, a Cu pseudopotential including 3rd shell states into the valence part is very steep. Hence, when working with a plane-wave basis, the usage of a PP of this kind may be computationally prohibitive.

On the other hand, the use of a pseudopotential without explicit treatment of 3d-electrons has been shown to be unreliable². Hence, first-principles methods based on plane-waves have been used only seldom to treat Cu². However, methods have been devised for the construction of softer pseudopotentials³⁻⁶, which make the inclusion of the 3rd shell in the valence more affordable. The price to be paid is that the construction and use of such pseudopotentials, which often display a very strong

l-nonlocality, is a quite delicate matter. In particular, the choice of a reference component⁷ and the transferability checks must be done with care. These difficulties are more than compensated by the simplicity and elegance of the plane-waves formalism in the subsequent calculations. In the present work, two possible choices for the Cu pseudopotential are explored, i.e: a) including 3s and 3p electrons into the frozen core (a quite standard choice), and b) including the full 3rd shell in the valence. Fully converged Density Functional Theory – Local Density Approximation (DFT-LDA) calculations are performed at 60 and 140 Ry cutoff, respectively for case a) and b).

The paper is organized as follows: in Section II we give the details of the construction of the pseudopotentials used throughout this work ; in Sections III and IV we present the ground state properties and bandstructure, respectively, obtained with the different pseudopotentials; finally, in Section V, we compare the theoretical absorption and electron energy loss spectra with the experimental data, including the effects of Local Fields and intraband transitions.

II. PSEUDOPOTENTIAL GENERATION

The Cu atom has the ground-state electronic configuration [Ar]3d¹⁰4s¹ (or [Ne]3s²3p⁶3d¹⁰4s¹). 4s and 3d eigenvalues are separated, in DFT-LDA, by less than 0.5 eV. It is then quite obvious that freezing all states but the 4s one into the atomic core (i.e., to neglect the polarization of the 3d electrons) cannot yield a good, transferable pseudopotential. On the other hand, inclusion of the 3d electrons into the valence (we call this a “3d” pseudopotential) yields a much slower convergence of plane-wave expansions, due to the steepness of the d-component of the PP. Unfortunately, the spatial superposition between the 3d and 3s or 3p states is quite large, despite the large

($\simeq 70$ eV) energy separation. Hence, an even more conservative and secure choice for the PP is to include all 3s, 3p and 3d electrons into the valence: in fact, 2p and 3s states are well separated, both spatially and energetically ($\simeq 800$ eV). This latter choice gives rise to a PP which is even harder than the “3d” one, and which will be referred to as a “3s” pseudopotential, yielding 19 valence electrons per atom.

Using the traditional pseudopotential generation scheme proposed by Bachelet, Hamann and Schlüter (BHS)⁷ yields PP whose d component converges very slowly in Fourier space, requiring to work at an energy cutoff of 200 rydbergs or more. However, PPs which converge at less than 100 Rydbergs can be constructed by using specially devised schemes as those of refs.^{3–6}. We choose to restrict to the class of *norm conserving* pseudopotentials, in order to avoid the additional numerical complications arising from the charge-state dependence of the PP of ref.³. Moreover, our choices in generating the PP are dictated not only by the need of a fast convergence of the PP in Fourier space, but also by that of optimizing the PP accuracy and transferability, a non-trivial task when also 3s and 3p states are included into the valence. In particular, the Hamann scheme⁸ (which does not try to optimize the Fourier space convergence at all) turned out to yield much more accurate and transferrable norm-conserving PPs, particularly when the whole 3rd shell is included into the valence.

Hence, we strictly follow the Hamann procedure (described in the appendix of ref.⁸) whenever it is possible, i.e. in all cases except for the d components. For the latter, we follow the Troullier–Martins⁶ scheme, which allows us to reduce significantly the number of plane-waves requested for convergence without losing too much in transferability. In all other cases (i.e. for the s and p components of both “3s” and “3d” pseudopotentials) we found the Hamann procedure to be more convenient, even at the cost of a slower Fourier space convergence, since the TM one yielded significantly worse results, and/or ghost states⁹ when the PP were used in the Kleinman–Bylander form¹⁰.

Another delicate point is the choice of a reference component, i.e. of a PP angular momentum component which is taken to be valid for every $l \geq 3$. Often, the $l=2$ component is chosen as a reference, simply because this makes calculations easier. This choice is sometimes lacking a physical justification, and can be dangerous, as it has been shown by some of us in the case of Sn¹¹. In the present case the $l=2$ reference had to be avoided anyway, since it yielded a much worse transferability than the $l=0$ or $l=1$ choices, and sometimes gave rise to ghost states in the KB form.

Several trials and tests with different cutoff radii have been done, in order to optimize the PP transferability without increasing too much the number of plane waves requested for convergence. Transferability tests included both the plot of logarithmic derivatives, and the explicit calculation of pseudoatom eigenvalues in some

excited electronic configuration (both neutral and positively charged).

Finally, since 3s and 3p states in the solid preserve their atomic configuration better than 3d ones, their explicit inclusion into the valence can sometimes be avoided, by considering only the effects of the non-linearity of the exchange-correlation potential¹². Hence, a third pseudopotential, with frozen 3s and 3p electrons but including non-linear core-corrections has also been considered, and will be referred to as the “3d+NLCC” PP. In the latter, the core charge is represented by the true one for $r \geq 0.5$ Bohrs, and by a Gaussian model charge for $r \leq 0.5$ Bohrs.

The resulting optimal cutoff radii and reference l -components, chosen for our “3d”, “3s”, and “3d+NLCC” pseudopotentials, are given in Table I.

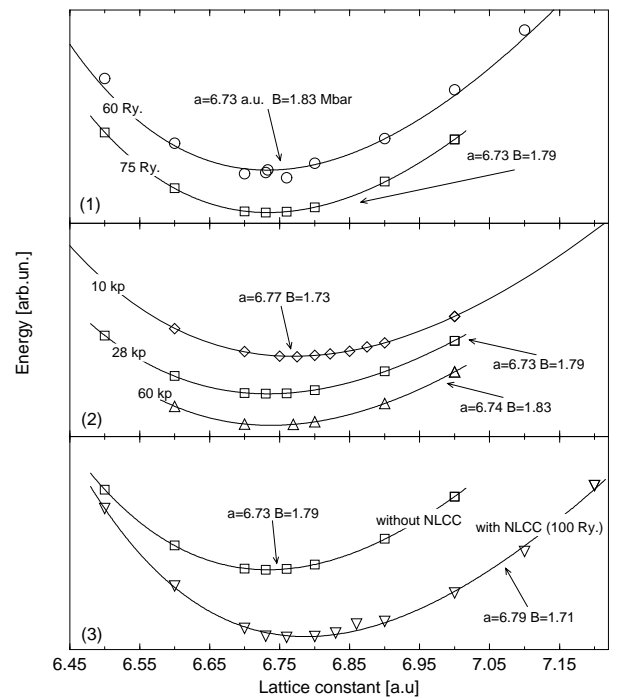


FIG. 1.: Calculated total energy vs. lattice constant for bulk Cu. Panel (1): effect of the kinetic energy cutoff at fixed number of k-points (28). Panel (2): effect of the IBZ sampling at fixed E_{cut} (75 Ry.); Panel (3): effect of nonlinear core-corrections (see text). The reported values for the equilibrium lattice constant and bulk modulus have been obtained from Murnaghan fits (continuous curves). The experimental values are $a=6.822$ Bohrs and $B=1.827$ MBar²⁹.

III. GROUND STATE PROPERTIES

Our first step is a self-consistent ground-state calculation, performed by minimizing the DFT–LDA energy functional with a Car–Parrinello method¹³, in a standard plane-wave basis. The Ceperley–Alder¹⁴ exchange–correlation energy and potential, as parametrized by

Perdew and Zunger¹⁵, have been used (test calculations with the Hedin–Lundqvist form¹⁶ have also been performed: see below). All our pseudopotentials are used within the fully–separable Kleinman–Bylander scheme¹⁰, after checking that no ghost–states was present⁹. The irreducible wedge of the Brillouin zone (IBZ) was sampled with the use of Monkhorst and Pack (MP) sets¹⁷ of N_k k–points. A very small fictitious electronic temperature (equal to ≈ 10 Kelvin) was used in order to accelerate the convergence of the calculated Fermi surface. Convergence with respect to both the k–points sampling and the kinetic energy cutoff has been checked extensively: Fig. 1 and Table II show the results obtained for the “3d” pseudopotential. $E_{cut} = 60$ Ry. and $N_k = 28$ appear to give well–converged, satisfactory results, with lattice constant a_0 and Bulk modulus B_0 within 1.4% of the experimental values. In the calculation with NLCC, the energy cutoff had to be increased to 100 Ry, in order to describe properly the core charge. NLCC reduce the underestimation of the experimental lattice constant to 0.5 %, but they are found to be almost influent on the bandstructure, as well as on the resulting spectra (see below). Finally, calculations with the “3s” pseudopotential, much deeper than the “3d” one, required an energy cutoff of 140 Ry. Also in this case, the effect on the LDA bandstructure and spectra in the energetic region of interest are found to be very small (see below).

In summary, as long as only the LDA 4s and 3d bandstructure is concerned, the effect of the inclusion of 3s and 3p in the valence, (as well as the use of NLCC), are mainly confined to a change of the equilibrium lattice constant, which induces an indirect effect on the bandstructure energies¹⁸.

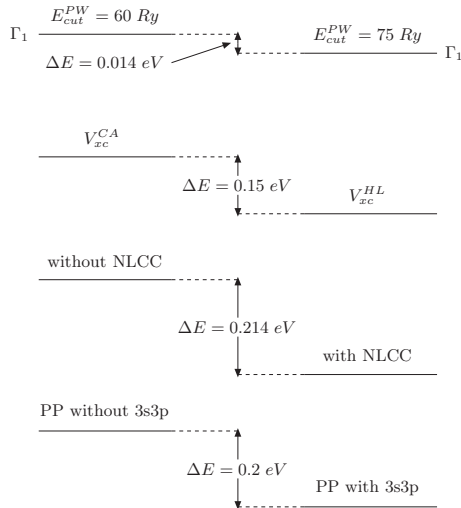


FIG. 2.: Summary of the effects of different computational details on the LDA bandstructure. The energy differences reported are the maximum ones, and correspond to the bottom valence band at the Γ point (Γ_1). They decrease gradually to zero at the Fermi level.

IV. LDA BAND STRUCTURE

Fig. 2 summarizes the maximum relative energy differences induced by different computational details on the LDA bandstructure; the value is taken at the bottom valence in the Γ point (Γ_1) and decreases gradually to zero at the Fermi level.

By changing E_{cut} from 60 Ry to 75 Ry the band-structure remains practically identical (changes are less than 0.02 meV). At the 60 Ry cutoff, we compare the band structure calculated with the Ceperley-Alder parametrization of the exchange–correlation potential^{14,15} with that obtained using the Hedin–Lunqvist parametrization¹⁶; in the latter case we find a maximum energy shift of about 0.15 eV.

The inclusion of NLCC yields, instead, a maximum upward shift of about 0.21 eV with respect to the case without NLCC, mainly due to the change in the equilibrium lattice constant. To study more deeply the effects of core polarization, we also performed a band-structure calculation with the “3s” pseudopotential (see Section II), where the 3s and 3p core level relaxation is fully included in the selfconsistent run. Also in this case the maximum bandshift with respect to the “3d” pseudopotential is limited to about 0.2 eV. Hence, our results obtained with the “3d” pseudopotential at $E_{cut}=60$ Ry. and using 28 MP k–points in the determination of the self–consistent charge density can be considered to represent the converged LDA bandstructure of bulk copper. Theoretical results are compared with the experimental photoemission data in Fig. 3.

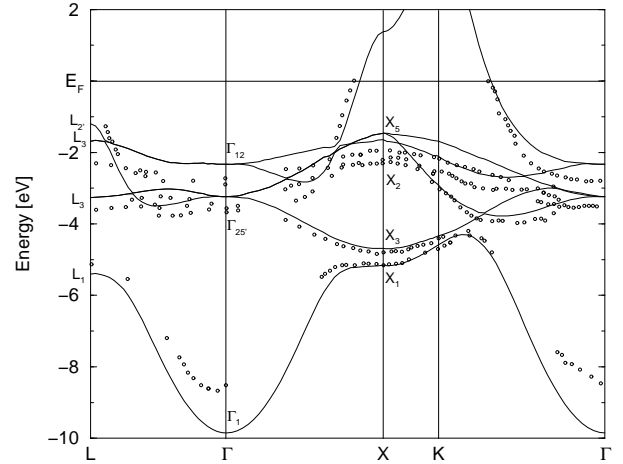


FIG. 3.: Bulk copper DFT-LDA bandstructure (full-line), compared with photoemission Data (points) from Ref. 1.

At difference with the case of semiconductors, the disagreement between theory and experiment is far from being limited to a rigid shift of the Kohn-Sham occupied eigenvalues with respect to the empty ones. In fact, as also summarized in Table III, the widths of the d bands

are systematically overestimated, a well-known failure of LDA when applied to transition and noble metals¹⁹.

V. ABSORPTION SPECTRUM

The absorption spectrum is given by the imaginary part of the macroscopic dielectric function:

$$\epsilon_M(\omega) = \frac{1}{\epsilon_{\mathbf{0}\mathbf{0}}^{-1}(\omega)}, \quad (1)$$

where

$$\epsilon_{\mathbf{0}\mathbf{0}}^{-1}(\omega) = 1 + \lim_{\mathbf{q} \rightarrow \mathbf{0}} \frac{4\pi}{|\mathbf{q}|^2} \chi_{\mathbf{G}=\mathbf{0} \mathbf{G}'=\mathbf{0}}(\mathbf{q}, \omega), \quad (2)$$

$\chi_{\mathbf{G} \mathbf{G}'}(\mathbf{q}, \omega)$ is the reducible polarization, solution of the equation

$$\chi_{\mathbf{G} \mathbf{G}'}(\mathbf{q}, \omega) = \chi_{\mathbf{G} \mathbf{G}'}^0(\mathbf{q}, \omega) + \sum_{\mathbf{G}''} \chi_{\mathbf{G} \mathbf{G}''}^0(\mathbf{q}, \omega) \frac{4\pi}{|\mathbf{q} + \mathbf{G}''|^2} \chi_{\mathbf{G}'' \mathbf{G}'}(\mathbf{q}, \omega). \quad (3)$$

Neglecting (for the moment) intraband transitions, $\chi_{\mathbf{G} \mathbf{G}''}^0(\mathbf{q}, \omega)$ is given by:

$$\chi_{\mathbf{G} \mathbf{G}'}^0(\mathbf{q}, \omega) = \frac{1}{2} \int_{BZ} \frac{d^3\mathbf{k}}{(2\pi)^3} \sum_{n \neq n'} \langle n' \mathbf{k} - \mathbf{q} | e^{-i(\mathbf{q} + \mathbf{G}) \cdot \mathbf{r}} | n \mathbf{k} \rangle \langle n \mathbf{k} | e^{i(\mathbf{q} + \mathbf{G}') \cdot \mathbf{r}'} | n' \mathbf{k} - \mathbf{q} \rangle \mathcal{G}_{he}^0(n, n', \mathbf{k}, \mathbf{q}, \omega), \quad (4)$$

with

$$\mathcal{G}_{he}^0(n, n', \mathbf{k}, \mathbf{q}, \omega) = f_{n'}(\mathbf{k} - \mathbf{q})(2 - f_n(\mathbf{k})) \left[\frac{1}{\omega + \epsilon_{n'}(\mathbf{k} - \mathbf{q}) - \epsilon_n(\mathbf{k}) + i\eta} - \frac{1}{\omega + \epsilon_n(\mathbf{k}) - \epsilon_{n'}(\mathbf{k} - \mathbf{q}) - i\eta} \right]. \quad (5)$$

with $0 \leq f_n(\mathbf{k}) \leq 2$ representing the occupation number summed over spin components. The sums over k are transformed to integrals over the BZ, and the latter are evaluated by summing over large sets of random points contained in the whole BZ. Fully converged calculations with a small broadening require a very large number of k -points²⁰; in the present work, the broadening used (and the corresponding number of k -points which was found to be sufficient to ensure convergence) is specified explicitly for each one of the reported spectra.

The simplest approach to the calculation of the absorption spectrum neglects the full inversion of Eq. (3) (i.e., neglects Local Field Effects), and assumes

$$\epsilon_M(\omega) \approx 1 - \lim_{\mathbf{q} \rightarrow \mathbf{0}} \frac{4\pi}{|\mathbf{q}|^2} \chi_{\mathbf{G}=\mathbf{0} \mathbf{G}'=\mathbf{0}}(\mathbf{q}, \omega). \quad (6)$$

The $\mathbf{q} \rightarrow \mathbf{0}$ limit for the oscillator strengths appearing in Eq. (4) is calculated in the transversal gauge²¹, within first order perturbation theory²²

$$\lim_{\mathbf{q} \rightarrow \mathbf{0}} \langle n' \mathbf{k} - \mathbf{q} | e^{-i\mathbf{q} \cdot \mathbf{r}} | n \mathbf{k} \rangle = -i\mathbf{q} \cdot \frac{\langle \phi_{n' \mathbf{k} - \mathbf{q}} | [\mathbf{r}, H] | \phi_{n \mathbf{k}} \rangle}{\epsilon_{n'}(\mathbf{k}) - \epsilon_n(\mathbf{k})} + O(q^2), \quad (7)$$

where $\phi_{n\mathbf{k}}(\mathbf{r})$ are the Bloch functions. Due to the non local character of the norm-conserving pseudopotentials, the well-known relation between $[\mathbf{r}, H]$ and the momentum operator

$$[\mathbf{r}, H] = \mathbf{p}. \quad (8)$$

must be substituted by:

$$[\mathbf{r}, H] = \mathbf{p} + [\mathbf{r}, V_{NL}]. \quad (9)$$

The second term of the rhs of Eq. (9), which in simple metals and in many semiconductors is small (and often neglected in practical calculations), becomes extremely important in the case of copper due to the large nonlocality of the PP.

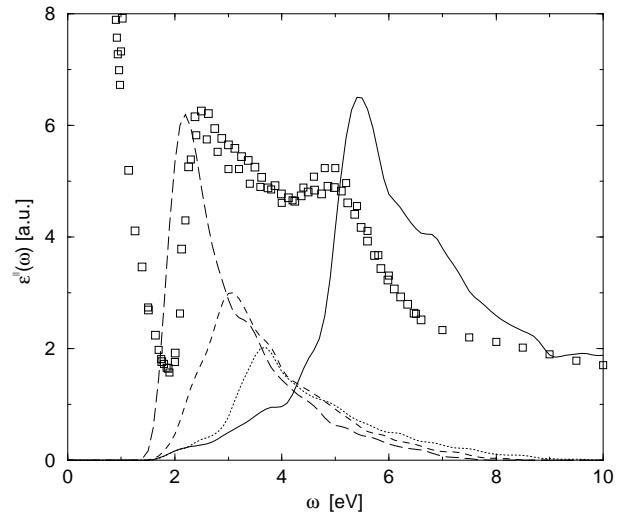


FIG. 4.: Full line: imaginary part of the macroscopic dielectric function of Cu without Local-Field effects and without including the non-local pseudopotential commutator [Eq. (9)], compared with experimental data (squares) from³⁰. Dot, dashed and long-dashed lines correspond to the functions defined in Eq. (10) with $n' = 3$, $n' = 4$ and $n' = 5$ respectively. All theoretical curves are computed with $N_k = 15,386$, and a Gaussian broadening of 0.15 eV (see text).

This is demonstrated in Fig. 4 where the imaginary part of ϵ_M is calculated assuming the validity of Eq. (8) The experimental absorption spectrum is severely underestimated between the offset of interband transitions

(≈ 1.74 eV) and 5 eV. A better analysis of this behavior can be performed by plotting the quantity

$$\Im m \left[\frac{\sum_{\mathbf{k}} \mathcal{G}_{he}^0(n, n', \mathbf{k}, \mathbf{0}, \omega)}{\omega^2} \right]. \quad (10)$$

with $n = 6$ and $n' = 3, 4, 5$ (see Fig. 4). This quantity is the joint density of states (JDOS) (divided by ω^2) for transitions between the sixth band (d -like) and the third to fifth bands (sp -like), and corresponds to assuming an oscillator strength equal to one in Eq. (4).

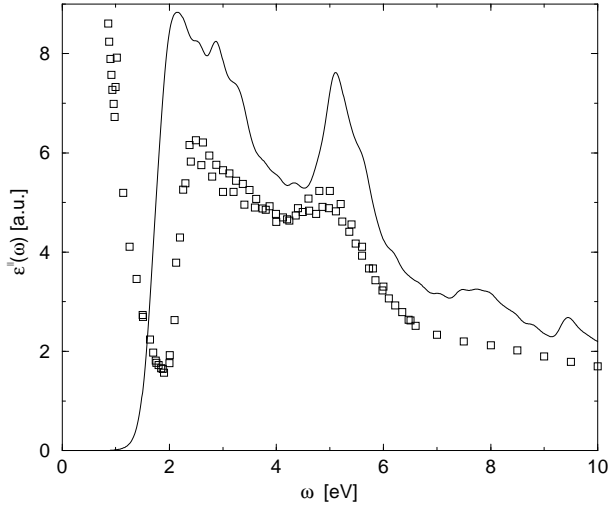


FIG. 5.: Full line: imaginary part of the macroscopic dielectric function of Cu without Local-Field effects and *including* the non-local pseudopotential commutator [Eq. (9)], compared with experimental data (squares)³⁰. N_k and broadening as in Fig. 4.

We see that transitions in the energy range of interest (1.8 to 5.0 eV) exist, but they are strongly suppressed due to the small values of the corresponding matrix elements of \mathbf{p} . Using both terms of Eq. (9), instead, we obtain the spectrum shown in Fig. 5, comparing much better with experiments. The large influence of the non-local pseudopotential commutator on $d \rightarrow sp$ optical transitions can be understood by writing explicitly the contribution of the second term of Eq. (9):

$$\langle \phi_{(s/p)\mathbf{k}} | [\mathbf{r}, V_{NL}] | \phi_{(d)\mathbf{k}} \rangle = \sum_{l=s,p,d} \iint d\mathbf{r} d\mathbf{r}' \phi_{(s/p)\mathbf{k}}^*(\mathbf{r}) [\mathbf{r} V_{NL}^l(\mathbf{r}, \mathbf{r}') - V_{NL}^l(\mathbf{r}, \mathbf{r}') \mathbf{r}'] \phi_{(d)\mathbf{k}}(\mathbf{r}'), \quad (11)$$

where $V_{NL}^l(\mathbf{r}, \mathbf{r}')$ is the l -orbital component of the pseudopotential, and $\phi_{(s/p)\mathbf{k}}(\mathbf{r})$, $\phi_{(d)\mathbf{k}}(\mathbf{r})$ are the s/p like and d like Bloch functions. Now we can approximate the sum

in Eq. (11) with the leading terms, to obtain:

$$\langle \phi_{(s/p)\mathbf{k}} | [\mathbf{r}, V_{NL}] | \phi_{(d)\mathbf{k}} \rangle \approx \iint d\mathbf{r} d\mathbf{r}' \left[\phi_{(s/p)\mathbf{k}}^*(\mathbf{r}) \mathbf{r} V_{NL}^d(\mathbf{r}, \mathbf{r}') \phi_{(d)\mathbf{k}}(\mathbf{r}') - \phi_{(s/p)\mathbf{k}}^*(\mathbf{r}) (V_{NL}^s(\mathbf{r}, \mathbf{r}') + V_{NL}^p(\mathbf{r}, \mathbf{r}')) \mathbf{r}' \phi_{(d)\mathbf{k}}(\mathbf{r}') \right]. \quad (12)$$

In the case of copper the d components of the pseudopotential differ from the p component near the origin by about 20 Hartrees, and this explain the strong influence on $\epsilon_M''(\omega)$.

Despite the strong improvement of the agreement with experiment obtained in Fig. 5, the theoretical curve exhibits an amplitude overstimulation of about 20% with respect to the experimental absorption spectrum.

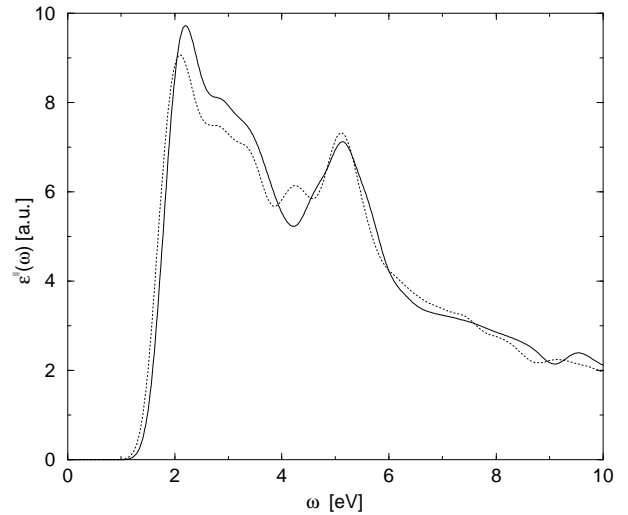


FIG. 6.: Effect of the use of a pseudopotential including the 3s and 3p shells in the valence on the calculated $\epsilon''(\omega)$ for bulk Cu (full line : “3d” PP; dotted line: “3s” PP. See text). Due to the large number of plane-waves required by the “3s” PP, the comparison is done using a small number of k -points and a relatively large Gaussian broadening ($N_k = 3,000$, $\gamma = 0.2$ eV). Local-Field effects are neglected, and Eq. (9) is used.

This drawback must be analyzed taking into account both the *physical approximations* involved in our theoretical approach, and the possible *residual errors* due to the PP scheme. Concerning the first ones, the most important point is the neglect of self-energy effects in the bandstructure calculation, and of excitonic effects in the absorption process. Concerning the PP scheme, instead, a possible reason for the overstimulation of the spectrum intensity could be related to the use of pseudo-wavefunctions instead of the all-electrons ones in Eq. (4). This effect has been studied in atoms by the authors of Ref.²³: they found that PP calculations, even when the second term of rhs of Eq. (9) is correctly taken into account, can be affected by a small residual error due to the

difference between all-electron wavefunctions and pseudo wavefunctions *inside the core region*. In the case of the Cu atoms, $3d \rightarrow 4p$ transitions were found to yield a matrix element which was too large by about 10%²³.

The effect of this overestimation of the $3d \rightarrow 4p$ intra-atomic optical matrix elements on the calculated bulk spectrum is, however, not obvious. To clarify this point, we have performed an accurate comparison of the results obtained by using the “3d” and “3s” pseudopotentials, both in case of the bulk crystal and for the isolated Cu atom. For the latter case, our results are summarized in Table IV: while our “3d” pseudopotential gives about the same results as those obtained in Ref.²³, the “3s” PP reduces the error on the intra-atomic optical matrix elements to less than 1.5 %. However in the case of the bulk crystal the amplitude of our calculated spectrum does not change appreciably when results obtained with “3d” and “3s” pseudopotentials are compared (see Fig. 6). This suggests that the overall intensity overestimation cannot be ascribed to the use of PP wavefunctions in Eq. (4).

The reason for this discrepancy between theory and experiment should hence be searched for within the physical approximations made, such as the neglect of self-energy effects that are currently under investigation and will be the subject of a forthcoming paper²⁴.

A. Intraband transitions

A peculiar characteristic of metals is the intra-band contribution to the dielectric function, which, neglecting local field effects, is given by:

$$\epsilon'_{intra}(\omega) \equiv 1 - \lim_{\mathbf{q} \rightarrow \mathbf{0}} \left\{ \frac{4\pi}{|\mathbf{q}|^2} \sum_n \int_{BZ} \frac{d^3\mathbf{k}}{(2\pi)^3} \right. \\ \left. [f_n(\mathbf{k} - \mathbf{q}) - f_n(\mathbf{k})] \frac{|\langle n\mathbf{k} | e^{i\mathbf{q}\cdot\mathbf{r}} | n\mathbf{k} - \mathbf{q} \rangle|^2}{\omega + \epsilon_n(\mathbf{k} - \mathbf{q}) - \epsilon_n(\mathbf{k})} \right\}, \quad (13)$$

with the n-sum restricted only to semi-occupied bands. In the case of copper only the sixth band contributes to Eq. (13). Indicating this band with n_F and using the relation

$$f_{n_F}(\mathbf{k} - \mathbf{q}) - f_{n_F}(\mathbf{k}) = (f_{n_F}(\mathbf{k} - \mathbf{q}) - f_{n_F}(\mathbf{k})) \\ \{ \theta [f_{n_F}(\mathbf{k} - \mathbf{q}) - f_{n_F}(\mathbf{k})] - \theta [f_{n_F}(\mathbf{k}) - f_{n_F}(\mathbf{k} - \mathbf{q})] \}, \quad (14)$$

time-reversal symmetry allows one to rewrite Eq. (13) as

$$\epsilon'_{intra}(\omega) \equiv 1 - \lim_{\mathbf{q} \rightarrow \mathbf{0}} \left\{ \frac{8\pi}{|\mathbf{q}|^2} \int_{BZ} \frac{d^3\mathbf{k}}{(2\pi)^3} \right. \\ \left. (f_{n_F}(\mathbf{k} - \mathbf{q}) - f_{n_F}(\mathbf{k})) \theta [f_{n_F}(\mathbf{k} - \mathbf{q}) - f_{n_F}(\mathbf{k})] \right. \\ \left. \frac{|\langle n\mathbf{k} | e^{i\mathbf{q}\cdot\mathbf{r}} | n\mathbf{k} - \mathbf{q} \rangle|^2 (\epsilon_{n_F}(\mathbf{k}) - \epsilon_{n_F}(\mathbf{k} - \mathbf{q}))}{\omega^2 - (\epsilon_{n_F}(\mathbf{k}) - \epsilon_{n_F}(\mathbf{k} - \mathbf{q}))^2} \right\}, \quad (15)$$

In the small \mathbf{q} limit, Eq. (15) yields the well-known Drude contribution to the dielectric function

$$\epsilon'_{intra}(\omega) \equiv 1 - \frac{\omega_D^2}{\omega^2} + O(q^2), \quad (16)$$

with

$$\omega_D^2 = \lim_{\mathbf{q} \rightarrow \mathbf{0}} \left\{ \frac{8\pi}{|\mathbf{q}|^2} \int_{BZ} \frac{d^3\mathbf{k}}{(2\pi)^3} \right. \\ \left. (f_{n_F}(\mathbf{k} - \mathbf{q}) - f_{n_F}(\mathbf{k})) \theta [f_{n_F}(\mathbf{k} - \mathbf{q}) - f_{n_F}(\mathbf{k})] \right. \\ \left. |\langle n\mathbf{k} | e^{i\mathbf{q}\cdot\mathbf{r}} | n\mathbf{k} - \mathbf{q} \rangle|^2 (\epsilon_{n_F}(\mathbf{k}) - \epsilon_{n_F}(\mathbf{k} - \mathbf{q})) \right\}. \quad (17)$$

Since the theta function in Eq. (17) limits strongly the region of BZ that contributes to the integral, the \mathbf{k} -space sampling and the modulus of the chosen \mathbf{q} vector used in the numerical evaluation of Eq. (17) become two critical convergence parameters: for a small $|\mathbf{q}|$ very few \mathbf{k} -points will satisfy the condition $[f_{n_F}(\mathbf{k} - \mathbf{q}) - f_{n_F}(\mathbf{k})] \neq 0$. In practice, $|\mathbf{q}|$ must be small enough to reproduce the $\mathbf{q} \rightarrow \mathbf{0}$ limit in Eq. (17), but large enough to allow a suitable number of \mathbf{k} -points to contribute to the sum. To obtain a well converged ω_D^2 we found it necessary to use $\approx 16,000$ random \mathbf{k} -points in a region of the BZ such that $\epsilon_{n_F}(\mathbf{k})$ is contained within $\epsilon_{Fermi} \pm 0.1$ eV. The value used was $|\mathbf{q}| = 0.005$ a.u.. A fictitious electronic temperature was introduced to smear out the Fermi surface, increasing the number of $(\mathbf{k}, \mathbf{k} - \mathbf{q})$ pairs giving non zero contributions to Eq. (17). In Table V we present our results as a function of the fictitious electronic temperature. The optical mass, defined as

$$m_{opt} = \left(\frac{\omega_c}{\omega_D} \right)^2 \quad \text{with} \quad \omega_c = \sqrt{\frac{4\pi}{\Omega}} = 10.8 \text{ eV} \quad (18)$$

with Ω direct lattice cell volume, converges to 1.36, a value in good agreement with the experiment²⁵.

B. Local field effects

Local-Field effects are accounted for when the macroscopic dielectric function is computed according to Eq. (1-3), i.e. by explicitly obtaining $\chi_{\mathbf{G}\mathbf{G}'}(\mathbf{q}, \omega)$ as

$$\chi_{\mathbf{G}\mathbf{G}'}(\mathbf{q}, \omega) = \chi_{\mathbf{G}\mathbf{G}'}^0(\mathbf{q}, \omega) \\ \left[1 - \frac{4\pi}{|\mathbf{q} + \mathbf{G}|^2} \chi_{\mathbf{G}\mathbf{G}'}^0(\mathbf{q}, \omega) \right]^{-1}, \quad (19)$$

We divide explicitly $\chi_{\mathbf{G}\mathbf{G}'}^0(\mathbf{q}, \omega)$ into intraband and interband contributions:

$$\chi_{\mathbf{G}\mathbf{G}'}^0(\mathbf{q}, \omega) = \chi_{\mathbf{G}\mathbf{G}'}^{inter}(\mathbf{q}, \omega) + \chi_{\mathbf{G}\mathbf{G}'}^{intra}(\mathbf{q}, \omega), \quad (20)$$

where the interband part is given by Eq. (4), while for the intraband contribution we have to evaluate:

$$\chi_{\mathbf{G}\mathbf{G}'}^{intra}(\mathbf{q}, \omega) = \frac{1}{2} \int_{BZ} \frac{d^3\mathbf{k}}{(2\pi)^3} \langle n_F \mathbf{k} - \mathbf{q} | e^{-i(\mathbf{q}+\mathbf{G})\cdot\mathbf{r}} | n_F \mathbf{k} \rangle \langle n_F \mathbf{k} | e^{i(\mathbf{q}+\mathbf{G}')\cdot\mathbf{r}'} | n_F \mathbf{k} - \mathbf{q} \rangle \mathcal{G}_{he}^0(n_F, n_F, \mathbf{k}, \mathbf{q}, \omega). \quad (21)$$

with $\mathcal{G}_{he}^0(n, n', \mathbf{k}, \mathbf{q}, \omega)$ defined in Eq. (5). For $G, G' \neq 0$ the oscillator strength is calculated using Fast Fourier Transforms (FFT)

$$\langle n\mathbf{k} - \mathbf{q} | e^{-i(\mathbf{q}+\mathbf{G})\cdot\mathbf{r}} | n'\mathbf{k} \rangle = \langle u_{n\mathbf{k}} | e^{-i\mathbf{G}\cdot\mathbf{r}} | u_{n'\mathbf{k}} \rangle + O(q), \quad (22)$$

while for the $G = G' = 0$ element of χ^{inter} we use Eq. 7.

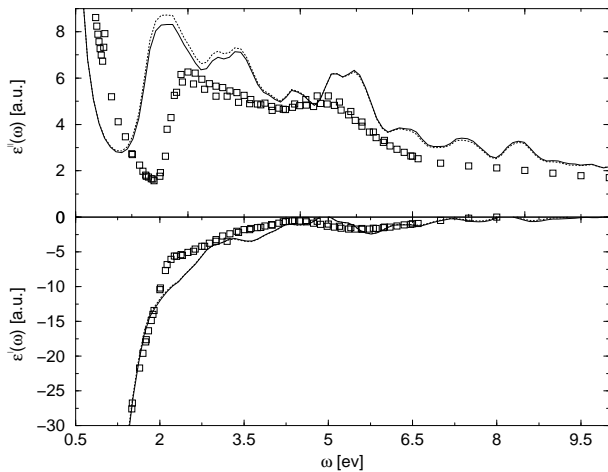


FIG. 7.: Real and imaginary part of $\varepsilon_M(\omega)$ for bulk Cu with (full line) and without (dotted line) inclusion of Local-Field effects, compared with experimental data (squares) from Ref.³⁰. Theoretical spectra are computed with $N_k = 110$ (in the irreducible wedge of BZ), and a Lorentzian broadening of 0.4 eV (see text).

The method presented in Section VA for the calculation of ω_D could, in principle, be extended to $\chi_{\mathbf{G}\mathbf{G}'}^{intra}(\mathbf{q}, \omega)$. Unfortunately the explicit calculation of χ^{intra} for all the $(\mathbf{G}, \mathbf{G}')$ pairs is computationally prohibitive, due to the large number of \mathbf{k} -points required to reach convergence. To overcome these difficulties, we have evaluated Eq. (21) on a limited number of \mathbf{k} -points (a MP grid of 110 points in the irreducible wedge). $\mathcal{G}_{he}^0(n_F, n_F, \mathbf{k}, \mathbf{q}, \omega)$ is different from zero only for \mathbf{k} very close to the Fermi Surface (which, in the grid, coincides with one particular point \mathbf{k}_F) where $f_{n_F}(\mathbf{k} - \mathbf{q})(2 - f_{n_F}(\mathbf{k})) \neq 0$. The oscillator strengths can be considered to be almost constant in the vicinity of the Fermi Surface. The same ansatz cannot be applied to $\mathcal{G}_{he}^0(n_F, n_F, \mathbf{k}, \mathbf{q}, \omega)$; however we can use the property that near the Fermi surface the metallic band dispersion of copper is well approximated by a free-metal one, and

make the following assumption for $\chi_{\mathbf{G}\mathbf{G}'}^{intra}(\mathbf{q}, \omega)$:

$$\chi_{\mathbf{G}\mathbf{G}'}^{intra}(\mathbf{q}, \omega) \approx \frac{1}{N_s} \left[\sum_{\mathbf{R}} \langle n_F \mathbf{R}\mathbf{k}_F - \mathbf{q} | e^{-i(\mathbf{q}+\mathbf{G})\cdot\mathbf{r}} | n_F \mathbf{R}\mathbf{k}_F \rangle \langle n_F \mathbf{R}\mathbf{k}_F | e^{i(\mathbf{q}+\mathbf{G}')\cdot\mathbf{r}'} | n_F \mathbf{R}\mathbf{k}_F - \mathbf{q} \rangle \right] \pi_0(\mathbf{q}, \omega), \quad (23)$$

where \mathbf{R} is one of the N_s symmetry operations not in the point group of \mathbf{k}_F . $\pi_0(\mathbf{q}, \omega)$ is the non-interacting polarization calculated for a jellium model²⁶ with a density n_{el} yielding a classic plasma frequency $\omega_p = \sqrt{4\pi n_{el}} = 9.27$ eV, corresponding to the value of ω_D calculated in Section VA.

$$\pi_0(\mathbf{q}, \omega) = -\frac{1}{2\pi^2|\mathbf{q}|} \int_0^{k_F^{jel}|\mathbf{q}|} x dx \left(\frac{1}{\omega - k_F^{jel}|\mathbf{q}| + i\eta} - \frac{1}{\omega - k_F^{jel}|\mathbf{q}| - i\eta} \right). \quad (24)$$

where

$$x = \frac{\omega}{k_F^{jel}|\mathbf{q}|}. \quad (25)$$

and

$$k_F^{jel} = (r\pi^2 n_{el})^{1/3}. \quad (26)$$

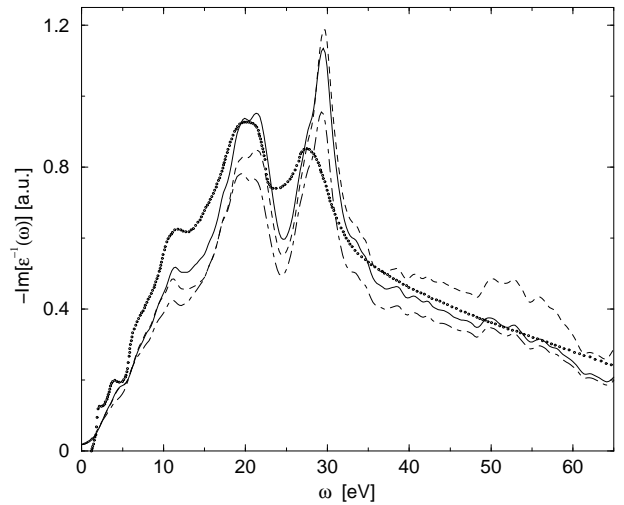


FIG. 8.: Imaginary part of the inverse macroscopic dielectric function of Cu including Local-Field effects and the Drude contribution (full line). Dashed line: results without Local-Field effects; Long-short dashes: with Local-Field effects, but without the Drude contribution. All theoretical spectra are computed with the same N_k of Fig. 7 but with a Lorentzian broadening of 0.9 eV. Points are the EELS data from Ref.³⁰.

In Fig. 7 we compare our results for $\varepsilon_M''(\omega)$ with and without Local Field Effects. The differences are small,

consistently with the fact that, as expected, no large LFE are present in a metal. However Local Field effects are more important on the EELS spectrum, as shown in Fig. 8: in the high energy region the full inversion of $\chi_{\mathbf{G}\mathbf{G}'}(\mathbf{q},\omega)$ matrix corrects an overestimation of the intensity. The inclusion of intraband transitions, on the other hand, turns out to be necessary not only to describe correctly the behaviour of ϵ'' at low frequencies, but also to improve the agreement of the calculated $\epsilon^{-1}(\omega)$ with the experimental EELS data (Fig.8).

VI. CONCLUSIONS

Several conclusions can be drawn from the presented results. First, we have shown that fully converged DFT-LDA calculations for bulk copper using plane waves can be performed without requiring an exceedingly large basis set, by using soft norm-conserving pseudopotentials including the 3d electrons in the valence.

The strong non-locality implied by such pseudopotentials reflects itself in a very large contribution of the commutator between the PP and the position operator in the calculation of the matrix elements entering the dielectric function.

Similar calculations including also the 3s and 3p shells in the valence are also feasible using plane waves, but show very little difference on the bandstructure and on the optical matrix elements not directly involving those shells.

At difference with the case of simple semiconductors, the disagreement between the LDA theoretical bandstructure and the experimental one cannot be corrected by a rigid shift of the Kohn-Sham eigenvalues: this suggests the importance of many body effects in the quasi-particle spectrum of Cu. These effects should be taken into account through a calculation including self-energy contributions²⁴. By contrast, the computed optical mass, which involves only intraband transitions at the Fermi energy, is in very good agreement with the experimental data. Also the theoretical absorption spectrum, where only LDA eigenvalues within a few eV around the Fermi energy are important, displays a quite satisfactory agreement with the experimental one. The overall overestimation of about 20 percent in the amplitude of the main peaks cannot be attributed to the effect of wavefunction pseudization *inside* the core region, and should be ascribed to the neglect of self-energy (and excitonic) effects. Finally, local field effects on the macroscopic dielectric function turn out to be negligible, with or without the inclusion of the Drude term.

ACKNOWLEDGMENTS

This work has been supported by the INFN PRA project "IMESS" and by the EU through the

NANOPHASE Research Training Network (Contract No. HPRN-CT-2000-00167). We thank L. Reining and A. Rubio for useful discussions. We are grateful to S. Goedecker for providing us an efficient code for Fast Fourier Transforms²⁷.

-
- ¹ R. Courths and S. Hüfner, Phys. Rep. **112**, 53 (1984).
 - ² I. Campillo, A. Rubio and J.M. Pitarke, Phys. Rev. B **59**, 12188 (1999).
 - ³ D. Vanderbilt, Phys. Rev. B **41**, 7892 (1990).
 - ⁴ A. M. Rappe, K. M. Rabe, E. Kaxiras, and J.D. Joannopoulos, Phys. Rev. B **41**, 1227 (1990).
 - ⁵ E.L. Shirley, D.C. Allan, R.M. Martin, and J. D. Joannopoulos, Phys. Rev. B **40**, 3652 (1989).
 - ⁶ N. Troullier and J.L. Martins, Phys. Rev. B **43**, 1993 (1991).
 - ⁷ G. Bachelet, D.R. Hamann and M. Schlüter Phys. Rev. B **26**, 4199 (1982).
 - ⁸ D. R. Hamann, Phys. Rev. B **40**, 2980 (1989).
 - ⁹ X. Gonze, P. Käckell, M. Scheffler, Phys. Rev. B **41**, 12264 (1990).
 - ¹⁰ I. Kleinman and D. M. Bylander, Phys. Rev. Lett. **48**, 1425 (1982).
 - ¹¹ M. Meyer, G. Onida, M. Palumbo and L. Reining, Phys. Rev. B **64**, 045119 (2001).
 - ¹² S. G. Louie, S. Froyen and M. L. Cohen, Phys. Rev. B **26**, 1738 (1982).
 - ¹³ R. Car and M. Parrinello, Phys. Rev. Lett. **55**, 2471 (1985).
 - ¹⁴ D.M. Ceperley and B.I. Alder, Phys. Rev. Lett. **45**, 566 (1980).
 - ¹⁵ J. P. Perdew and A. Zunger, Phys. Rev. B **23**, 5048 (1981).
 - ¹⁶ L. Hedin and B. I. Lundqvist, J. Phys. C. **4**, 2064 (1971).
 - ¹⁷ H. J. Monkhorst and J. D. Pack, Phys. Rev. B **13**, 5188 (1976).
 - ¹⁸ However, as long as we are interested in bare LDA result, the overall effect on the 3d - 4s bandstructure and on the absorption spectrum is small and, a posteriori, we can simply use our "3d" PP.
 - ¹⁹ R. O. Jones and O. Gunnarsson, Rev. Mod. Phys. **61**, 689 (1989).
 - ²⁰ S. Albrecht, L. Reining, G. Onida, V. Olevano and R. Del Sole, Phys. Rev. Lett. **83**, 3971 (1999).
 - ²¹ R. Del Sole and R. Girlanda, Phys. Rev. B **48**, 11789 (1993).
 - ²² M. S. Hybertsen and S. G. Louie, Phys. Rev. B **35**, 5585 (1987).
 - ²³ J. Read and R.J. Needs, Phys. Rev. B **44**, 13071 (1991).
 - ²⁴ A. Marini, R. Del Sole and G. Onida, unpublished.
 - ²⁵ H. Ehrenreich and H.R. Philipp, Phys. Rev. **128**, 1622 (1962).
 - ²⁶ R. D. Mattuck, *A guide to Feynman diagrams in the Many-Body problem*, McGraw-Hill, New York (1976) p. 196-200.
 - ²⁷ S. Goedecker, Comp. Phys. Commun. **76**, 294 (1993); SIAM Journal on Scientific Computing **18**, 1605 (1997).
 - ²⁸ M. Bockstedte, A. Kley, J. Neugebauer, M. Scheffler, Com-

put. Phys. Comm. **107**, 187 (1997).

²⁹ R.W.G. Wyckoff, *Crystal Structure*, 2nd ed., Interscience, New York (1976).

³⁰ E.D. Palik, *Handbook of Optical Constants of Solids* (Academic Press, New York, 1985).

Pseudopotential	r_s [Bohr]	r_p [Bohr]	r_d [Bohr]	Reference l-component
“3d”	1.19 (H)	1.19 (H)	2.08 (TM)	s
“3d+NLCC”	1.10 (H)	1.19 (H)	2.08 (TM)	s
“3s”	0.49 (H)	0.60 (H)	1.19 (TM)	p

TABLE I. Cu Pseudopotential cutoff radii and reference components. (H) and (TM) stand for Hamann (ref.⁸) and Troulliers–Martins (ref.⁶) schemes, respectively. All our pseudopotentials are norm-conserving in the sense of Bachelet, Hamann and Schlüter⁷, and have been produced using a publicly available Fortran code²⁸. They are also available in numerical form upon request by e-mail to: onida@roma2.infn.it

PW cutoff (Ry)	Nk	a_0 [Bohr]	B_0 [MBar]
75	10	6.77	1.73
75	28	6.73	1.79
75	60	6.74	1.83
60	28	6.73	1.83
100+NLCC	28	6.79	1.71
Expt.	–	6.82	1.83

TABLE II. Convergence of the calculated ground-state properties of bulk Cu.

		Experiment ¹	Present work
positions of d-bands	Γ_{12}	–2.78	–2.33
	X_5	–2.01	–1.46
	L_3	–2.25	–1.69
widths of d-bands	$\Gamma_{12} - \Gamma_{25'}$	0.81	0.91
	$X_5 - X_3$	2.79	3.23
	$X_5 - X_1$	3.17	3.70
	$L_3 - L_3$	1.37	1.58
	$L_3 - L_1$	2.91	3.72
positions of sp-bands	Γ_1	–8.60	–9.85
	$L_{2'}$	–0.85	–1.12
L-gap	$L_1 - L_{2'}$	4.95	4.21

TABLE III. Comparison of Cu band widths and energy position with experimental values¹ at high-symmetry points. All energies in eV.

Optical transitions	AE	“3d” PP	“3s” PP
$4s \rightarrow 4p$	1.732	1.738	1.713
$3d \rightarrow 4p$	0.406	0.453	0.412

TABLE IV. Optical matrix elements for the Cu atom, calculated in the All-electrons (AE) scheme, and with the pseudopotentials used in the present work. Values are in atomic units.

T_{el} [eV]	Number of intraband transitions	ω_D [ev]	m_{opt}
0.1	14,617	9.39	1.32
0.01	2,456	9.41	1.32
0.001	534	9.25	1.36
0.0001	310	9.28	1.36
0.00001	296	9.27	1.36

TABLE V. Cu Drude plasma frequency and optical mass values obtained using different fictitious electronic temperatures; the experimental value for m_{opt} is 1.35²⁵.